VLF/ELF Radiation Patterns of Arbitrarily Oriented Electric and Magnetic Dipoles in a Cold Lossless Multicomponent Magnetoplasma

T. N. C. WANG

Radio Physics Laboratory, Stanford Research Institute
Menlo Park, California 94025

T. F. BELL

Radioscience Laboratory, Stanford University
Stanford, California 94305

With the use of a power integral formulation, a study is made of the VLF/ELF radiation patterns of arbitrarily oriented electric and magnetic dipoles in a cold lossless multicomponent magnetoplasma. Expressions for the ray patterns are initially developed that apply for arbitrary values of driving frequency f, static magnetic-field strength B_0, plasma density, and composition. These expressions are subsequently specialized to VLF/ELF radiation in a plasma modeled on the magnetosphere. A series of representative pattern plots are presented for frequencies between the proton (f_{pH}) and electron (f_{eH}) gyrofrequencies. These patterns illustrate the fact that focusing effects that arise from the geometrical properties of the refractive index surface tend to dominate the radiation distribution over the entire range $f_{eH} \geq f \geq 4.6 f_{pH}$. Focusing effects are particularly strong in the range $\frac{1}{2} f_{eH} \geq f \geq f_{LHR}$, where the major lobe of the pattern lies along B_0 and the lobe intensity varies inversely as the first power of the distance between source and observer rather than as the square of this distance. It is concluded that focusing effects should be of significant importance in the design of a VLF/ELF satellite transmitting system in the magnetosphere.

In recent years there has been a great interest on the part of the geophysical scientific community in the idea of a satellite-based VLF/ELF transmitter that would operate in the magnetosphere. Such a transmitter would provide a means of performing a number of important and interesting experiments involving wave-particle interactions, wave-propagation phenomena, and space-plasma diagnostics. In addition, the transmitter could also serve as part of a VLF communication system. The usefulness of this VLF transmitter in performing experimental tasks will be limited ultimately by the amount and distribution of power that can be radiated into the magnetoplasma from the antennas. The details of the radiation pattern are especially important if the satellite transmitter is a low-power device, since then the possibility of generating waves of useful amplitude may depend on maximizing the flow of power at a given wave-normal direction.

A first-order estimate of the VLF radiation patterns of electric or magnetic dipole antennas in the magnetosphere can be obtained by assuming this plasma to be cold, uniform, and infinite in extent. These idealizations have been used extensively by previous workers to evaluate the far fields of simple antennas in a magnetoplasma, but the resultant medium is still so complicated that the fields can only approximately be found through the use of saddle-point integration techniques.

To the authors' knowledge, very little discussion of the radiation pattern of a magnetic dipole antenna in a magnetoplasma has appeared in the literature [*GiaRusso and Bergeson*, 1970; *Wu*, 1963; *Wang and Bell*, 1969*a*]. On the other hand, the specific problem of the far fields radiated from an electric antenna has been considered by a number of workers [*Bunkin*, 1957; *Kuehl*, 1962; *Mittra and Deschamps*, 1963; *Arbel and Felsen*, 1963; *Wu*, 1963; *Kogelnik and Motz*, 1963; *Freire and Scarabucci*, 1967; *Mittra and Duff*, 1965; *Wang and Bell*, 1969*a*; *GiaRusso and Bergeson*, 1970]. In their works, all these authors have attacked the problem by employing the usual definition of the time-averaged poynting vector

with the asymptotic fields obtained from the saddle-point evaluations. Since the number of saddle points depends on the point of observation and since higher-order saddle points usually appear, the study of the antenna radiation pattern using the time-averaged poynting vector turns out to be considerably complicated. In most of these early papers, very little numerical data have been presented regarding the VLF radiation pattern of dipole antennas in a plasma similar to the magnetosphere. Furthermore, no explicit forms for the ray pattern are given except for the uniaxial case [*Freire and Scarabucci*, 1967].

Recently *GiaRusso and Bergeson* [1970] used *Kuehl's* [1962] method to calculate the radiation pattern for electric and magnetic dipoles for various frequencies in the VLF frequency range; however, their work suffers from an error that becomes serious in the lossless case and invalidates their results for frequencies between the lower-hybrid-resonance frequency and approximately one-half the electron gyrofrequency.

In the present paper, we investigate the VLF/ELF radiation pattern of both electric and magnetic dipoles embedded in a cold collisionless uniform multicomponent magnetoplasma. In this study we make use of an integral expression of real radiated power and appropriate saddle-point relations. This alternative method for calculation of the radiation pattern has been qualitatively described in an earlier paper by *Staras* [1964], and it is found to be a somewhat simpler way of obtaining the ray pattern than the usual poynting-vector approach. Corrections to this method are necessary when higher-order saddle points appear, and in these cases we present a simple technique for joining the first-order and second-order saddle-point results. Our final radiation-pattern plots consequently include all focusing effects that arise from the geometrical properties of the refractive-index surfaces.

BASIC METHOD FOR CALCULATION OF RADIATION PATTERN

When a time-harmonic current source is immersed in a medium, the total time-averaged complex power is formally given by

$$P = -\frac{1}{2}\int \mathbf{E}(-\mathbf{k})\cdot\mathbf{J}^*(\mathbf{k})\,d\mathbf{k} \qquad (1)$$

For a lossless dielectric medium, it is known that the real part and the imaginary part of (1) represent the radiated power and the stored energy (reactive power), respectively. Generally, one can write (1) in terms of spherical-polar coordinates for the wave vector $\mathbf{k}$ and then perform a contour integration with respect to the variable k ($k = |\mathbf{k}|$, the magnitude of $\mathbf{k}$) to obtain P as double integral involving the polar and azimuthal angles of $\mathbf{k}$. With the real part of this expression, the total real power output can then formally be written

$$P_r = \int_{\psi,\theta} f(\psi, \theta)\sin\theta\,d\theta\,d\psi \qquad (2)$$

where θ and ψ are the polar angle and the azimuthal angle for the wave vector $\mathbf{k}$, respectively.

For the case of a lossless system, (2) is then a representation of total real radiated power summed up from the rays in the wave-normal space. In terms of observation coordinates, one may generally use a set of relations

$$\begin{aligned}\theta &= \theta(\gamma, \phi)\\ \psi &= \psi(\gamma, \phi)\end{aligned} \qquad (3)$$

and write (2) as

$$P_r = \sum_i \int f'(\gamma, \phi)\frac{\partial(\theta, \psi)}{\partial(\gamma, \phi)}\sin\gamma\,d\gamma\,d\phi \qquad (4)$$

where the 'i' summation covers the relevant branches of the functions given in (3); γ and ϕ are the polar and azimuthal angles in the observation space; $f'(\gamma, \phi)$ stands for $[f(\psi, \theta)](\sin\theta/\sin\gamma)$, with θ and ψ expressed in terms of γ and ϕ; and where $\partial(\theta, \psi)/\partial(\gamma, \phi)$ is the Jacobian of the transformation, given by $[\partial(\theta, \psi)/\partial(\gamma, \phi)] = |(\partial\theta/\partial\gamma)(\partial\psi/\partial\phi) - (\partial\theta/\partial\phi)(\partial\psi/\partial\gamma)|$. From (4), it is clear that in a lossless system the mean radiated power flux per unit solid angle in the observation coordinates, or the so-called "radiation-intensity" pattern, is given by the following expression:

$$\Gamma(\gamma, \phi) = \sum_i f'(\gamma, \phi)\frac{\partial(\theta, \psi)}{\partial(\gamma, \phi)} \qquad (5)$$

with the subsidiary conditions given by (3).

The subsidiary conditions of (3) are closely related to the properties of the dispersion surfaces, or refractive index surfaces, of the characteristic modes excited in the system [*Light-*

hill, 1960; *Arbel and Felsen*, 1963; *Felsen*, 1965; *Mittra and Duff*, 1965], and they can generally be identified as 'saddle-point' relations in the asymptotic evaluation of the far-zone fields.

For a cold magnetoplasma medium, if the polar axis in the wave-normal space is chosen to be parallel to the direction of the static magnetic field, the refractive indices of the characteristic modes are independent of ψ. In this situation, (3) reduces to the form

$$\begin{aligned} \theta &= \theta(\gamma) \\ \psi &= \phi + \phi_0 \end{aligned} \tag{6}$$

where $\phi_0 = 0$ or π for each saddle point. Equation 5 then becomes

$$\Gamma(\gamma, \phi) = \sum_i f'(\gamma, \phi) \left|\frac{\partial \theta}{\partial \gamma}\right| \tag{7}$$

Equations 6 and 7 represent the general form of the radiation pattern function in a cold lossless magnetoplasma. In the subsequent sections, we work out the explicit forms of (6) and (7) for the radiation from either an electric dipole or a magnetic dipole.

Saddle-Point Relations

GiaRusso and Bergeson [1970] gave a concise description of *Kuehl*'s [1962] method for formulating the exact electromagnetic fields radiated by sources in a cold magnetoplasma and indicated how these fields can be found approximately by using saddle-point–integration techniques involving a scalar integral function of the coordinates $I(r, r')$. For point sources radiating at frequencies between the proton and electron gyrofrequency in a relatively dense magnetoplasma, it can be shown [*Wang and Bell*, 1969*a*] that $I(r, r')$ has the form

$$I(\bar{r}) = \int_0^{\pi/2, \theta_r} L(\theta) J_0[\beta \mu(\theta) \rho] \cdot \exp\left[-j\beta v(\theta)\,|z|\right] \sin\theta\, d\theta \tag{8}$$

where $L(\theta)$ is a function of θ alone, J_0 is the zero-order Bessel function of the first kind, β equals the free space wave number, ρ and z are the respective transverse and axial components of $\mathbf{r}$ in spherical coordinates (i.e., ρ equals $r \sin\gamma$ and z equals $r \cos\gamma$), $\mu(\theta)$ equals $n(\theta) \sin\theta$, $v(\theta)$ equals $n(\theta) \cos\theta$, and the whistler-mode refractive index $n(\theta)$ has the form

$$n(\theta) = \frac{(\epsilon_{+1}\epsilon_{-1} - \epsilon_0\epsilon_s)\sin^2\theta + 2\epsilon_0\epsilon_s - q(\theta)}{2(\epsilon_0 \cos^2\theta + \epsilon_s \sin^2\theta)} \tag{9}$$

where

$$q(\theta) = [(\epsilon_0\epsilon_s - \epsilon_{+1}\epsilon_{-1})^2 \sin^4\theta + 4\epsilon_0^2\epsilon_d^2 \cos^2\theta]^{1/2}$$

Notation not defined above is defined in other papers [*Wang and Bell*, 1969*a*, *b*]. In (8) the upper limit $\pi/2$ applies to situations in which the wave frequency ω lies between the proton gyrofrequency ω_{pH} and the lower-hybrid-resonance frequency ω_{LHR}. Over this frequency range, the whistler-mode refractive-index surface is closed. The upper limit θ_r applies to instances in which ω lies between the electron gyrofrequency ω_{eH} and ω_{LHR}. Over this frequency range, the whistler-mode refractive-index surface is open in the lossless case and approaches infinity along the surface of a 'resonance' cone of half angle $\theta_r = \tan^{-1}|\epsilon_0/\epsilon_s|$.

To apply the saddle-point method to (8), it is assumed that the observation point is located far enough from the source so that we have $\beta rn \gg 1$ and that $L(\theta)$ is a slowly varying function of θ over the range of integration. Given these assumptions, two cases must then be distinguished, $\gamma \approx 0$ and $\gamma \not\approx 0$.

Case 1, $\gamma \approx 0$. If we have $\gamma \cong 0$, the observation point lies close to the static magnetic-field line that intersects the source. Since the argument of the Bessel function in (9) is now small, we can set $J_0 \sim 1$ in the integrand and the relation for the Sth-order saddle point becomes

$$\begin{aligned} \frac{\partial^i v(\theta)}{\partial \theta^i} &= 0 \qquad i = 1, \cdots, s \\ \frac{\partial^{s+1} v(\theta)}{\partial \theta^{s+1}} &\neq 0 \end{aligned} \tag{10}$$

By using the relation for $n(\theta)$ and assuming a relatively dense plasma (i.e., $\omega_0^2/\omega_{eH}^2 \gg 1$), it can be shown that, for frequencies in either of the two ranges $\omega_{eH} > \omega > \omega_{eH}/2$ and $\omega_{LHR} > \omega > \omega_{pH}$, there exists but one first-order saddle point that contributes to the radiation at $\gamma \sim 0$. This saddle point is located at $\theta = 0$. On the other hand, for frequencies in the range $\omega_{eH}/2 > \omega > \omega_{LHR}$, the radiation at $\gamma \sim 0$ is due to the contributions of two first-order saddle points,

$\theta_1 = 0$ and $\theta_2 = \cos^{-1}(2\epsilon_s/\epsilon_d)$. The presence of the saddle point θ_2 results in a focusing of radiation along the static magnetic-field-line direction such that the radiated energy drops off as r^{-1} rather than as the usual r^{-2}. Thus this saddle point is quite important in evaluating the far-field radiation pattern. As $\omega \to \omega_{eH}/2$, θ_1 and θ_2 merge with an additional saddle point to form a third-order saddle point that also represents focused radiation.

A detailed discussion of these focusing effects, as well as expressions for the axial field components, can be found in a previous paper [*Wang and Bell,* 1969*a*]; these expressions were used in preparing our pattern plots.

In formulating their expressions for the poynting flux, *GiaRusso and Bergeson* [1970] do not consider the case $\gamma \approx 0$, and consequently their results do not apply to radiation along the static magnetic field. To obtain values for this longitudinal flux, these authors have used an expression given by *Snyder and Weitzner* [1968] for the fields at $\gamma \approx 0$. Unfortunately the results of Snydor and Weitzner are not correct, since they have neglected to include the important saddle point θ_2 in their saddle-point calculation of the fields at $\gamma \approx 0$. Thus the results of GiaRusso and Bergeson are also incorrect at $\gamma \approx 0$, and the important effects of longitudinal focusing are overlooked by these authors.

An idea of the serious error involved in neglecting the longitudinal focusing can be obtained by noting that this focusing effect produces the major lobe in the dipole radiation patterns when $\omega_{LHR} \leq \omega \leq \frac{1}{2}\,\omega_{eH}$.

Case 2, $\gamma \neq 0$. When the argument of the Bessel function in (8) is large, the asymptotic form of the Bessel function can be used and (8) becomes

$$I(\bar{r}) = [2\pi\beta r \sin\gamma]^{-1/2}[I_+ + I_-] \tag{11}$$

where

$$I_\pm = \exp(\mp j\pi/4) \int_0^{\pi/2,\theta_r} L(\theta)[n(\theta)]^{-1/2} \cdot \exp[-j\beta r\psi_\pm(\theta,\gamma)]\, d\theta \tag{12}$$

and $\psi_\pm(\theta,\gamma) = n(\theta)\cos(\gamma \pm \theta)$.

In this case, the relations for the sth-order saddle points become

$$\frac{\partial^i}{\partial\theta^i}\psi_\pm(\theta,\gamma) = 0 \qquad i = 1, \cdots, s$$
$$\frac{\partial^{s+1}}{\partial\theta^{s+1}}\psi_\pm(\theta,\gamma) \neq 0 \tag{13}$$

The first-order saddle-point condition gives the relations between θ and γ necessary to complete (7)

$$\pm\gamma = \theta - \tan^{-1}(n'(\theta)/n(\theta)) \tag{14}$$

and

$$\left|\frac{\partial\theta}{\partial\gamma}\right| = \left|\frac{n^2(\theta) + [n'(\theta)]^2}{n^2(\theta) + 2[n'(\theta)]^2 - n(\theta)n''(\theta)}\right| \tag{15}$$

where the primes indicate a derivative with respect to θ. In principle, (15) can be used in (7) to construct radiation patterns for given sources in the plasma. However, if the whistler-mode refractive surface at a given frequency possesses a point of inflection (points where two first-order saddle points merge, i.e., a second-order saddle point), at the wave-normal angle θ_m appropriate to the inflection point it will be found from (15) that $|\partial\theta/\partial\gamma| \to \infty$. The equation relating the observation polar angle γ_m and the wave-normal angle θ_m at the inflection points can be deduced from (13) with $s = 2$

$$\gamma_m = \theta_m + \tan^{-1}\left[\frac{n(\theta_m) - n''(\theta_m)}{2n'(\theta_m)}\right] \tag{16}$$

where θ_m is real, less than $\pi/2$ in magnitude and satisfies the equation

$$n^2(\theta_m) + 2[n'(\theta_m)]^2 = n(\theta_m)n''(\theta_m) \tag{17}$$

In the high density limit ($\omega_0^2/\omega_H^2 \gg 1$), the following can be shown: (*a*) when $\omega_{LHR} > \omega \gtrsim 4.6\,\omega_{pH}$, the whistler-mode refractive-index surface $\bar{n}(\theta)$ possesses eight points of inflection (two in the range $0 \leq \theta \leq \pi/2$); (*b*) when $4.6\,\omega_{pH} > \omega \geq \omega_{pH}$ and when $\omega_{eH} \geq \omega > \omega_{eH}/2$, $\bar{n}(\theta)$ possesses no points of inflection; (*c*) when $\omega_{eH}/2 > \omega \geq \omega_{LHR}$, $\bar{n}(\theta)$ possesses four points of inflection (one in the range $0 \leq \theta \leq \theta_r$); and (*d*) when $\omega = \omega_{eH}/2$, $\bar{n}(\theta)$ possesses two third-order saddle points as described above in case 1. When $\omega \cong 4.6\,\omega_{pH}$, $\bar{n}(\theta)$ possesses four third-order saddle points (one in the range $0 \leq \theta \leq \pi/2$).

The presence of inflection points on the refractive-index surface results in a focusing of

radiation toward the observation point such that the radiated energy drops off as $r^{-5/2}$ instead of r^{-2} [*Arbel and Felsen*, 1963]. Since the power integral method fails at points of inflection and higher-order saddle points, it is necessary to supply additional relations to continue the radiation-pattern plots through these singular points.

A double saddle-point evaluation of an integral equivalent to (12) was made by *Arbel and Felsen* [1963] for the situation in which two first-order saddle points coalesce, and the expression they derive can be used to obtain the radiation pattern near γ_m. However, in view of the complexity of their results and the narrow angular range for which they are useful, we prefer to adopt an alternate scheme as outlined below.

From (14*d*), (16), and (17) of *Arbel and Felsen* [1963], we derive the following condition on the derivatives of $\psi(\theta)$ for which our single-saddle-point relation 15 is a good approximation

$$(\partial^2\psi/\partial\theta^2)^2 \gg (2/\beta r)^{2/3}(\partial^3\psi/\partial\theta^3)^{4/3} \qquad (18)$$

Equations 18 and 14 can be used to define a range of wave-normal angles for which the single-saddle-point technique is valid. Starting from any angle in this range, it can be shown that as $\theta \to \theta_m$ (θ_m is the angle at which the inflection point occurs), the right-hand side of (18) will eventually become approximately equal to the left, and, when this occurs, the double-saddle-point results of *Arbel and Felsen* [1963] can be used. For closer approach to θ_m, i.e., $\theta \approx \theta_m$, the inequality in (18) reverses and a second-order saddle-point technique is appropriate.

Since by assumption the quantity $\beta r\psi$ is a large number, (18) will generally be satisfied for angles within a few degrees of θ_m.

We now define implicitly two angles of 'closest approach' to θ_m by means of (14) and the relation

$$(\partial^2\psi/\partial\theta^2) = \pm(20/\beta r)^{1/3}(\partial^3\psi/\partial\theta^3)^{2/3} \qquad (19)$$

The real angles θ_r that satisfy (19) also satisfy (18) approximately, and thus the energy flow at θ_r can be treated by means of the first-order saddle-point relations 14 and 15. The two angles of interest in (19) are the two real roots that minimize the quantity $|\theta_r - \theta_m|$. By expanding the left-hand side of (19) in a Taylor series about θ_m, it can be shown that these two angles are given approximately by the relation

$$\theta_r - \theta_m \cong \pm(20/\beta r)^{1/3}(\partial^3\psi/\partial\theta^3)_{\theta=\theta_m}^{-1/3} \qquad (20)$$

The wave-normal angles θ_m and θ_r are associated with angles γ_m and γ_r in the observation space. The ratio of the power flux flowing in the direction γ_m to that flowing in the direction γ_r can be deduced from the results of *Arbel and Felsen* [1963, equations 10 and 18]

$$F = \frac{[\Gamma(1/3)]^2}{3(3)^{\frac{1}{2}}\pi} |\psi''| \, |\psi'''|^{-2/3} \left(\frac{\beta r}{2}\right)^{1/3} \qquad (21)$$

where $\Gamma(x)$ is the well-known gamma function and where all quantities are to be evaluated at $\theta = \theta_r$.

The radiation pattern of an arbitrary source in the magnetoplasma can now be found in the following way. First we define a distance from the source to the observation point. The power integral method (equations 4, 7, 14, and 15) is then used for all angles θ that satisfy equation 18, including angles θ_r. The exact value of the power flux at γ_m is then obtained by multiplying the power flux at γ_r by the 'focusing factor' F. Points lying in the narrow interval between γ_r and γ_m are approximated by fitting a smooth curve between the known values of the power flux at γ_r and γ_m, with the maximum of the curve at γ_m.

Since the focusing factor F depends only on the properties of the whistler-mode refractive-index surface and the distance to the observation point, plots of F versus frequency and distance that will apply to an arbitrary source in the plasma can be prepared. Similarly, plots of θ_m, θ_r, γ_m, and γ_r versus f and r that will apply to an arbitrary source in the plasma can also be prepared. Although we used such plots in preparing our radiation patterns, for the sake of brevity they are not presented here.

RADIATION PATTERNS

Electric dipole. Using the formulation developed by the authors in a previous paper [*Wang and Bell*, 1969*b*], we obtain the total power radiated into the half space $z > 0$ at fixed frequency in a cold magnetoplasma by an arbitrarily oriented infinitesimal electric dipole of unit moment

$$P_r = C_E \sum_{s=\pm} \int_0^{2\pi} d\psi \int_{\theta_s} [F_\parallel^s(\theta) \cos^2 \gamma_0 + F_\perp^s(\theta, \psi) \sin^2 \gamma_0] \sin \theta \, d\theta \quad (22)$$

where the θ_s integration covers all angles in the range $0 \leq \theta \leq \pi/2$ for which each of the magnetoionic modes ($s = \pm$) is propagating, γ_0 is the angle between the dipole axis and the static magnetic field, $C_E = \beta^4 c^2 Z_0/32\pi^2$, $c \cong 3 \times 10^8$ m/sec, and $Z_0 \cong 377$ ohms and where

$$F_\parallel^{\pm}(\theta) = \mp \frac{n_\pm^3 (n_\pm^2 - \epsilon_{+1})(n_\pm^2 - \epsilon_{-1})}{q(\theta)(n_\pm^2 - \epsilon_0)} \cdot \cos^2 \theta$$

$$F_\perp^{\pm}(\theta, \psi) = \mp \frac{n_\pm (n_\pm^2 - \epsilon_0)}{q(\theta)} \cdot \left[\cos^2 \psi + \frac{\epsilon_d^2}{(n_\pm^2 - \epsilon_{+1})(n_\pm^2 - \epsilon_{-1})} \right] \sin^2 \theta \quad (23)$$

In (23) the function $n_\pm$ represents the refractive indices of the two characteristic modes that exist in the cold magnetoplasma; remaining notation is defined by *Wang and Bell* [1969*a*, *b*]. For frequencies between the proton and electron gyrofrequency, only the whistler mode (n_-) is propagating (if a moderately dense plasma is assumed), and the radiation pattern (obtained from equations 22, 2, 4, and 7) has the form

$$\Gamma(\gamma, \phi) = C_E[\Gamma_\parallel(\gamma) \cos^2 \phi_0 + \Gamma_\perp(\gamma, \phi) \sin^2 \phi_0] \quad (24a)$$

$$\Gamma_\parallel(\gamma) = \sum F_\parallel^-(\gamma) \frac{\sin \theta}{\sin \gamma} \left| \frac{\partial \theta}{\partial \gamma} \right| \quad (24b)$$

$$\Gamma_\perp(\gamma, \phi) = \sum F_\perp^-(\gamma, \phi) \frac{\sin \theta}{\sin \gamma} \left| \frac{\partial \theta}{\partial \gamma} \right| \quad (24c)$$

where $\partial\theta/\partial\gamma$ is defined in (15), the summation in (24) includes all physically acceptable branches of $\theta(\gamma)$ (obtained from equation 14), $F_\parallel^-(\gamma)$ is $F_\parallel^-[\theta(\gamma)]$, and $F_\perp^-(\gamma, \phi)$ equals $F_\perp[\theta(\gamma), \psi = \phi]$.

Magnetic dipole. Using a previously developed formulation [*Wang and Bell*, 1969*b*, 1972], we obtain the total power radiated into the half space $z > 0$ at fixed frequency in a cold magnetoplasma by an arbitrarily oriented infinitesimal magnetic dipole of unit moment

$$P_r = C_M \sum_{s=\pm} \int_0^{2\pi} d\psi \int_{\theta_s} [L_\parallel^s(\theta) \cos^2 \gamma_0 + L_\perp^s(\theta, \psi) \sin^2 \gamma_0] \sin \theta \, d\theta \quad (25)$$

where the θ_s integration covers all angles in the range $0 \leq \theta < \pi/2$ for which each of the magnetoionic modes is propagating, γ_0 is the angle between the dipole axis and the static magnetic field, $C_M = \beta^4 Z_0/32\pi^2$, and where

$$L_\parallel^{\pm}(\theta) = \mp \frac{\epsilon_d^2 n_\pm^5 (n_\pm^2 - \epsilon_0)}{q(\theta)(n_\pm^2 - \epsilon_{+1})(n_\pm^2 - \epsilon_{-1})} \sin^2 \theta$$

$$L_\perp^{\pm} = \left[\mp \frac{n_\pm^5 (\epsilon_0 - \epsilon_{+1})(\epsilon_0 - \epsilon_{-1})}{q(\theta)(n_\pm^2 - \epsilon_0)} \cdot \sin^2 \theta \sin^2 \psi + L_\parallel^{\pm}(\theta) \right] \cos^2 \theta \quad (26)$$

Other notation in (26) is defined by *Wang and Bell* [1969*a*, *b*]. For $\omega_{pH} \leq \omega \leq \omega_{eH}$, only the whistler mode can propagate and the ray pattern, as obtained from (26), (2), (4), and (7), can be written

$$\Gamma(\gamma, \phi) = C_M[\Gamma_\parallel(\gamma) \cos^2 \gamma_0 + \Gamma_\perp(\gamma, \phi) \sin^2 \gamma_0] \quad (27a)$$

where

$$\Gamma_\parallel(\gamma) = \sum L_\parallel^-(\gamma) \frac{\sin \theta}{\sin \gamma} \left| \frac{\partial \theta}{\partial \gamma} \right| \quad (27b)$$

$$\Gamma_\perp(\gamma, \phi) = \sum L_\perp^-(\gamma, \phi) \frac{\sin \theta}{\sin \gamma} \left| \frac{\partial \theta}{\partial \gamma} \right| \quad (27c)$$

In (27), $\partial\theta/\partial\gamma$ is defined as in (15), the summation includes all physically acceptable branches of $\theta(\gamma)$, $L_\parallel^-(\gamma) \equiv L_\parallel^-[\theta(\gamma)]$, and $L_\perp^-(\gamma, \phi) \equiv L_\perp^-[\theta(\gamma), \psi = \phi]$.

NUMERICAL RESULTS

From the analysis of the preceding section, it is evident that the radiation pattern of an arbitrarily oriented point dipole can be expressed through the relation $\Gamma(\gamma, \phi) = \Gamma_\parallel(\gamma, \phi) \cos^2 \gamma_0 + \Gamma_\perp(\gamma, \phi) \sin^2 \gamma_0$, where γ_0 is the angle between the static magnetic field $\bar{B}_0$ and the axis of symmetry of the dipole and where $\Gamma_\parallel(\gamma, \phi)$ and $\Gamma_\perp(\gamma, \phi)$ are the radiation patterns of the dipole when its axis is oriented parallel or perpendicular to $\bar{B}_0$. In view of this relation, it is sufficient to plot only $\Gamma_\parallel(\gamma, \phi)$ and $\Gamma_\perp(\gamma, \phi)$ as a function of frequency in the VLF range. The

radiation pattern for values γ_0 between 0 and $\pi/2$ can then be constructed from the plots.

Since our main concern is to show the relative spatial distribution of the radiated power for a fixed signal frequency, the numerical curves for the ray patterns are normalized. The ray patterns for the electric dipole are normalized by the factor C_E (f_0/f), and those of the magnetic dipole are normalized by the factor $C_M(f_0/f)^3$, where f_0 is the plasma frequency of the magnetoplasma.

We attempted to arrange the radiation plots in such a way as to emphasize common characteristics. This arrangement led naturally to a classification based on the type and number of saddle points (rays) that contribute to the radiation pattern at any given normalized wave frequency f/f_{eH}. Generally, the type and number of contributing saddle points depend on the normalized plasma frequency f_0/f_{eH} as well as the normalized wave frequency, but, in the event that the plasma density ranges from moderate to high so that $(f_0/f_{eH})^2 \gg 1$, it can be shown that the relative distribution of radiated energy at any given frequency is substantially independent of the plasma frequency. Since the condition $(f_0/f_{eH})^2 \gg 1$ holds throughout most of the inner magnetosphere, we chose to simplify our pattern classification by considering only this high density limit where the patterns are independent of f_0 and where the plasma density enters into the radiation pattern only through the pattern-normalization constants mentioned above.

Consequently, although our patterns are plotted for a value of density $f_0 = 5f_{eH}$, they will apply to all higher densities as well. Furthermore, in most instances we would expect the patterns to be reasonably accurate for densities as low as $f_0 \cong 2f_{eH}$.

An interesting feature of all the dipole radiation patterns over the frequency range $f_{eH} \geq f \geq f_{LHR}$ (Figures 1, 2, and 3) is the fact that the radiation amplitude approaches infinity on the surface of a cone of half angle γ_c whose axis lies along the static magnetic-field direction. The angle γ_c is complementary to the so-called 'resonance cone' half angle $\theta_r = \tan^{-1}|\epsilon_0/\epsilon_s|$ on which the whistler-mode refractive-index surface approaches infinity, and the cone of half angle γ_c will be denoted here as the 'complementary cone.' *Arbel and Felsen* [1963] gave a thorough description of the qualitative behavior of the radiation intensity near the complementary cone and showed that the details of the radiation pattern there depend strongly on the physical configuration of the source function. In particular, these authors show that in the lossless case, infinite values of radiation intensity are found at γ_c when the source function is represented as a point dipole, but that, when more physically reasonable descriptions of the source function are used, the radiation intensity may actually vanish at γ_c. In view of this finding, it is clear that the values of radiation intensity near γ_c shown on our plots have little, if any, physical significance. Consequently, we do not choose to refer to the radiation spikes near γ_c as major lobes in the radiation pattern, even though they do represent radiation maximums on our plots. The actual determination of the radiation intensity near γ_c would require a much more detailed calculation than we are able to present here, and the results would depend on the full details of the source function as well as on any loss processes that might exist in the plasma.

As discussed in the section on saddle-point relations, the presence of focusing effects results in a radiation pattern that is a function of distance from the source, in the sense that the relative amplitude of the focused beam increases with this distance. In preparing our plots, we assumed that the radial distance r between source and observation point is such as to satisfy the relation $(2\pi f_0/c)\ r \equiv r_0 = 5000$. This number for r_0 was chosen to be consistent with a scale height of about 1000 km for the plasma parameters and with a local plasma frequency of about 250 kHz. If one wishes to use the plots in instances in which r_0 will have some other value, it is only necessary to make use of the fact that, in the high density limit, the amplitude of the beam due to 'inflection point' focusing will vary as $(f_0r)^{1/3}$, whereas the amplitude of the longitudinally focused beam will vary as (f_0r) [*Wang and Bell*, 1969*a*].

For simplicity, we plotted the dipole patterns in only two planes: the plane that contains the z axis and the dipole axis ($\phi = 0$) and the plane that contains the z axis but is perpendicular to the dipole axis ($\phi = \pi/2$). The pattern for other azimuthal angles ϕ can be readily obtained from (24) and (27).

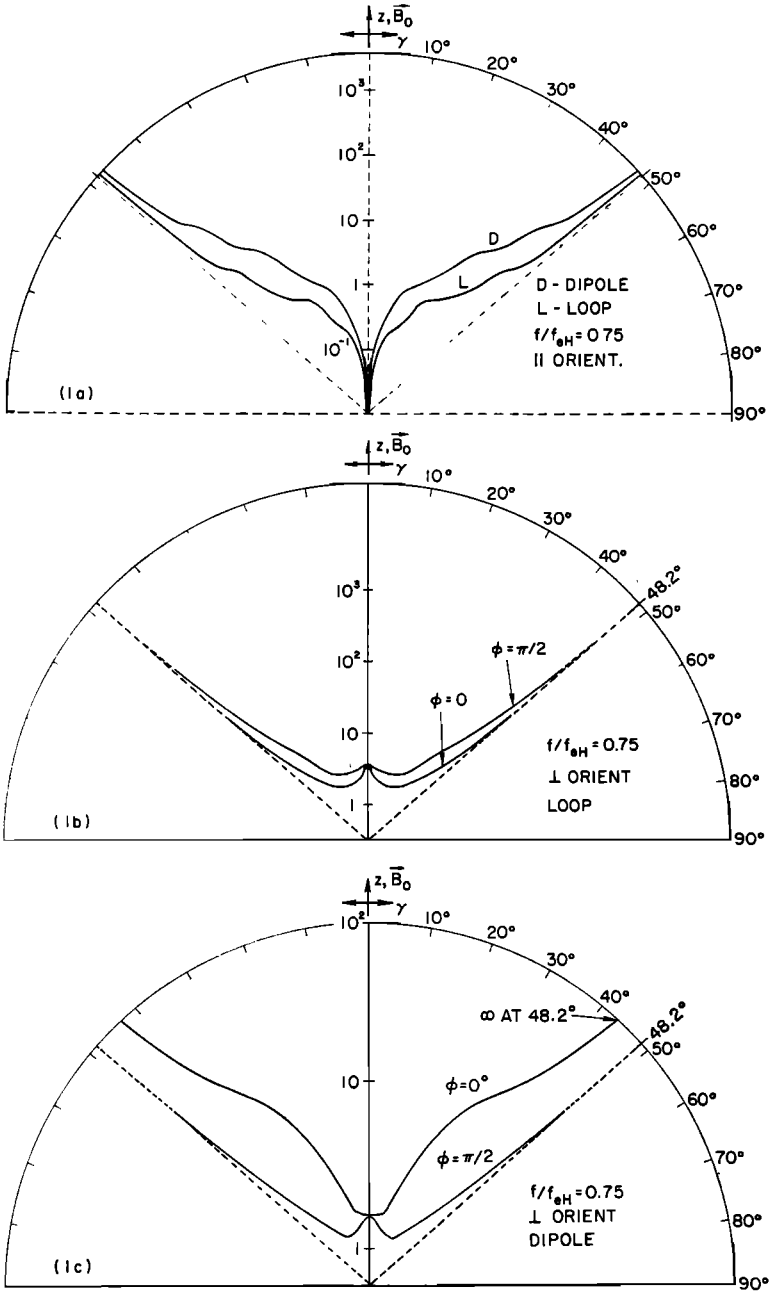

Fig. 1. Normalized radiation patterns for magnetic (L) and electric (D) dipoles at the frequency $f = 0.75\ f_{eH}$. The patterns shown are typical of those that occur in the frequency range $f_{eH} > f > \frac{1}{2}\ f_{eH}$, assuming a moderate to high density plasma.

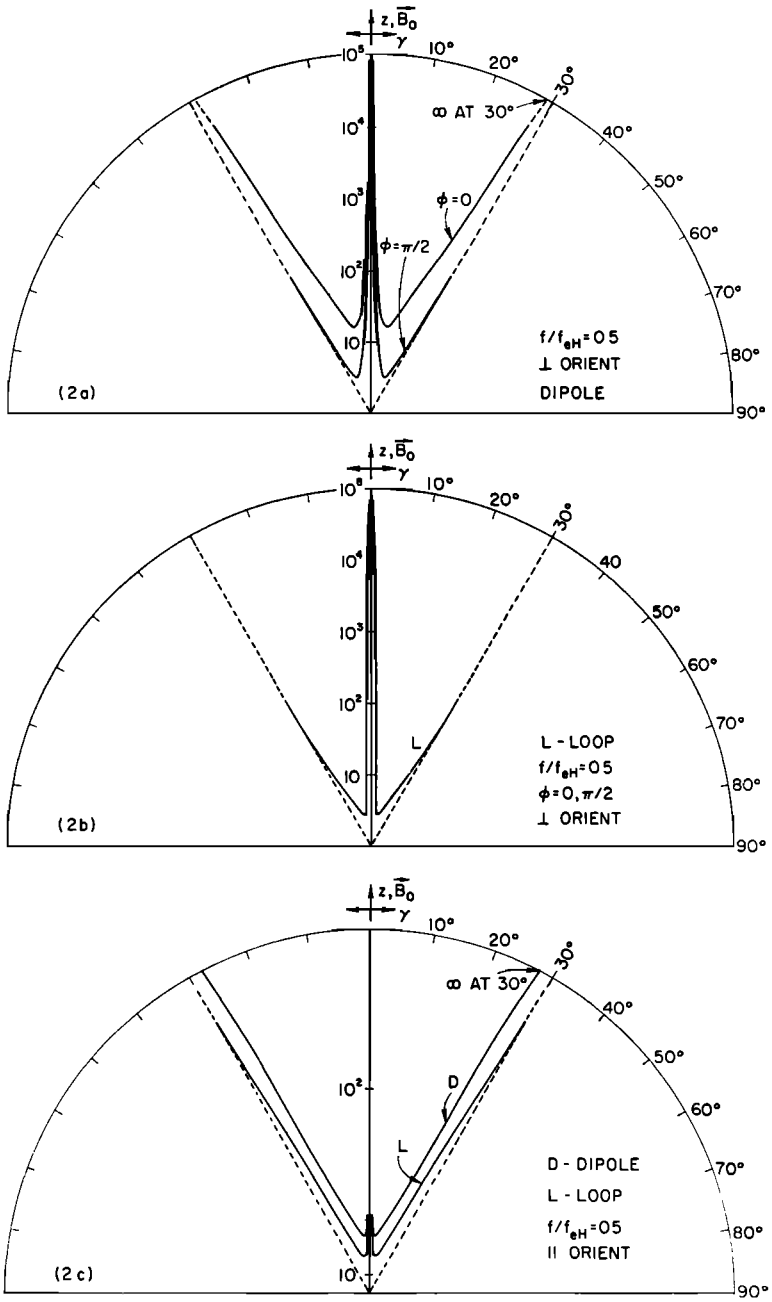

Fig. 2. Normalized radiation patterns for magnetic (L) and electric (D) dipoles at the frequency $f = \frac{1}{2} f_{eH}$. At this frequency the effects of longitudinal focusing are most pronounced and the major lobe of the pattern generally lies along $\bar{B}_0$. An exception occurs when the dipole symmetry axis lies exactly along $\bar{B}_0$ (as in Figure 2c) since the pattern null along $\bar{B}_0$ cancels out the focusing effect.

Although (24) and (27) are valid for a plasma of arbitrary composition, for present purposes we specialized to a two-component plasma consisting of equal numbers of electrons and protons.

The normalized radiation patterns for both magnetic and electric dipoles at a frequency $f = 0.75\, f_{eH}$ are shown in Figure 1. These plots illustrate the type of radiation pattern that occurs for frequencies in the range $\frac{1}{2} f_{eH} < f < f_{eH}$. In this frequency range, only one saddle point contributes to the radiation pattern, most of the radiated energy flows at an angle with respect to the static magnetic-field lines $\mathbf{B}_0$, and very little energy flows directly along $\mathbf{B}_0$. A typical refractive-index surface in this frequency range is shown in Figure 7*a*. From Figure 1*a* it is evident that the patterns for both electric dipoles (*D*) and magnetic dipoles (*L*) are fairly similar when the dipole axes are parallel to $\mathbf{B}_0$. Comparison of Figure 1*b* (magnetic dipole) with *c* (electric dipole) also indicates a reasonable similarity of radiation pattern for the situation in which the magnetic and electric dipole axes are perpendicular to $\mathbf{B}_0$, although the pattern for the electric dipole displays more variation as a function of azimuth about $\mathbf{B}_0$. In all instances the pattern amplitude is unbounded along the cone of half angle $\gamma_c = 48.2°$, i.e., the complementary cone. For angles $\pi/2 \geq \gamma > \gamma_c$, no radiation appears; thus for these frequencies the surface of the complementary cone represents a shadow boundary [*Arbel and Felsen*, 1963] for the radiation pattern.

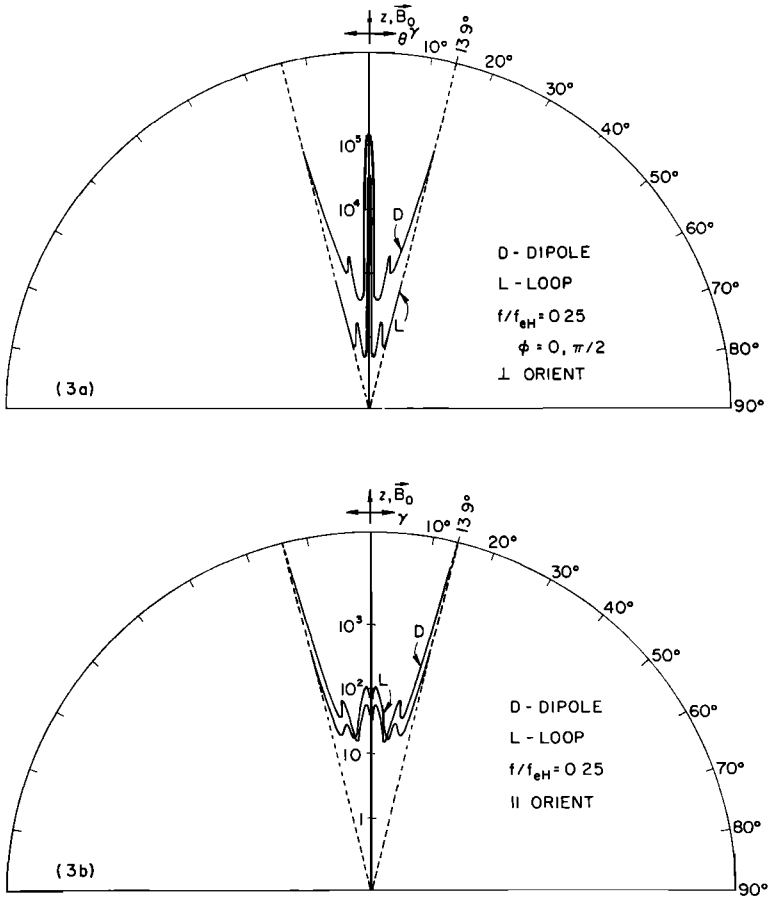

Fig. 3. Normalized radiation patterns for magnetic (*L*) and electric (*D*) dipoles at the frequency $f = 0.25\, f_{eH}$. The patterns shown are typical of those that occur in the frequency range $\frac{1}{2} f_{eH} > f \geq f_{LHR}$, assuming a moderate to high density plasma. Longitudinal focusing effects dominate the patterns in this frequency range.

The normalized radiation patterns for both magnetic and electric dipoles at the frequency $f = \frac{1}{2} f_{eH}$ are shown in Figure 2. At this frequency the effects of longitudinal focusing are most pronounced, and in general the major lobe of the radiation patterns lie along $\bar{B}_0$. This intense focusing is due to the presence of a third-order saddle point at $\theta = 0$ (when $\gamma = 0$). The focusing effect is clearly seen in Figure 2*a* (perpendicular electric dipole) and especially in *b* (perpendicular magnetic dipole), where almost the entire radiation output is contained in the center lobe. In Figure 2*c*, on the other hand, the focusing effect is counterbalanced by the fact that in a magnetoplasma neither an electric dipole (*D*) or a magnetic dipole (*L*) can radiate directly along their symmetry axis when that axis is parallel to $\bar{B}_0$. This null in the pattern at $\gamma = 0$ effectively suppresses the focusing effect and only a minor enhancement in the radiation appears near $\gamma \approx 0$. It is interesting to note that the pattern for the perpendicular magnetic dipole (Figure 2*b*) is essentially independent of azimuth about $\bar{B}_0$, whereas the pattern for the perpendicular electric dipole (Figure 2*a*) is a strong function of azimuth for $\gamma > 10°$. For this frequency, γ_c equals 30° and no radiation is present at larger angles.

The normalized radiation patterns for magnetic and electric dipoles at the frequency $f = \frac{1}{4} f_{eH}$ are shown in Figure 3. These plots are illustrative of the type of radiation pattern that occurs for frequencies in the range $f_{LHR} \leq f < \frac{1}{2} f_{eH}$. A typical refractive-index surface in this frequency range is shown in Figure 7*b*. In this frequency range, as many as three first-order saddle points can contribute to the radiation pattern, and one of these saddle points produces a strong focusing of radiation along $\bar{B}_0$. This focusing results in a pattern in which a major lobe lies along $\bar{B}_0$. Figure 3*a* clearly shows the effects of this longitudinal focusing for both perpendicular electric dipoles (*D*) and perpendicular magnetic dipoles (*L*). In Figure 3*a* a second lobe, somewhat weaker than that along $\bar{B}_0$, can be seen at $\gamma_m \sim 10°$. This secondary lobe results from radiation focusing that is due to the presence of inflection points on the whistler-mode refractive-index surface, and γ_m is given by (16). At this particular frequency, the secondary lobe lies within the complementary cone of half angle γ_c (equal to 13.9°) on which the radiation amplitude approaches infinity. For lower frequencies as $f \to f_{LHR}$, it is found that $\gamma_c \to 0$ whereas $\gamma_m \neq 0$. Thus the secondary lobe will lie outside the complementary cone, and the shadow boundary for the pattern is then represented by the cone of half angle γ_m about $\bar{B}_0$. It is not difficult to show that the half angle of the shadow-boundary cone reaches a minimum value when γ_c equals γ_m. This minimum occurs when $f \sim 0.2\ f_{eH}$, and the shadow-boundary–cone half angle here is approximately 11° [*Helliwell*, 1965, chapter 3]. An interesting feature of the patterns for the perpendicular dipoles is their symmetry about $\bar{B}_0$. For the parallel dipoles, Figure 3*b* shows that in this frequency range the longitudinal focusing effect is still strong in spite of the pattern null at $\gamma = 0$.

The normalized dipole radiation patterns for the frequency $f = 7 \times 10^{-3}\ f_{eH}$ are given in Figure 4. These plots are illustrative of the type of radiation pattern that occurs in the frequency range $4.6\ f_{pH} < f < f_{LHR}$. In this range as many as three first-order saddle points can contribute to the radiation pattern, and two major lobes are produced as a result of inflection points on the whistler-mode refractive-index surface. A typical refractive-index surface in this frequency range is shown in Figure 7*c*. In this frequency range, there is no focusing of radiation along $\bar{B}_0$. Furthermore, the whistler-mode refractive-index surface is closed, and no complementary cone exists; consequently, there are no forbidden regions for radiation. Comparing Figure 4*a* and *d* (magnetic dipole) with Figure 4*b* and *c* (electric dipole), it can be seen that the radiation patterns of the magnetic and electric dipoles have little similarity in any orientation. Not only are the pattern shapes different, but the variation with azimuth is different as well.

The normalized dipole radiation patterns for the frequency $f = 2.5 \times 10^{-3}\ f_{eH}$ ($f = 4.6\ f_{pH}$) are depicted in Figure 5. For this frequency only one saddle point contributes to the radiation pattern, and no longitudinal focusing takes place. The major lobe located at $\gamma = 24.5°$ is the result of focusing that is due to a third-order saddle point that was produced by the merging of two inflection points on the whistler-mode refractive index surface. This focusing causes the lobe amplitude to increase as $r^{1/2}$. By comparing Figure 5*a* and *c* (magnetic dipole) with Figure 5*b* and *d* (electric dipole), it is

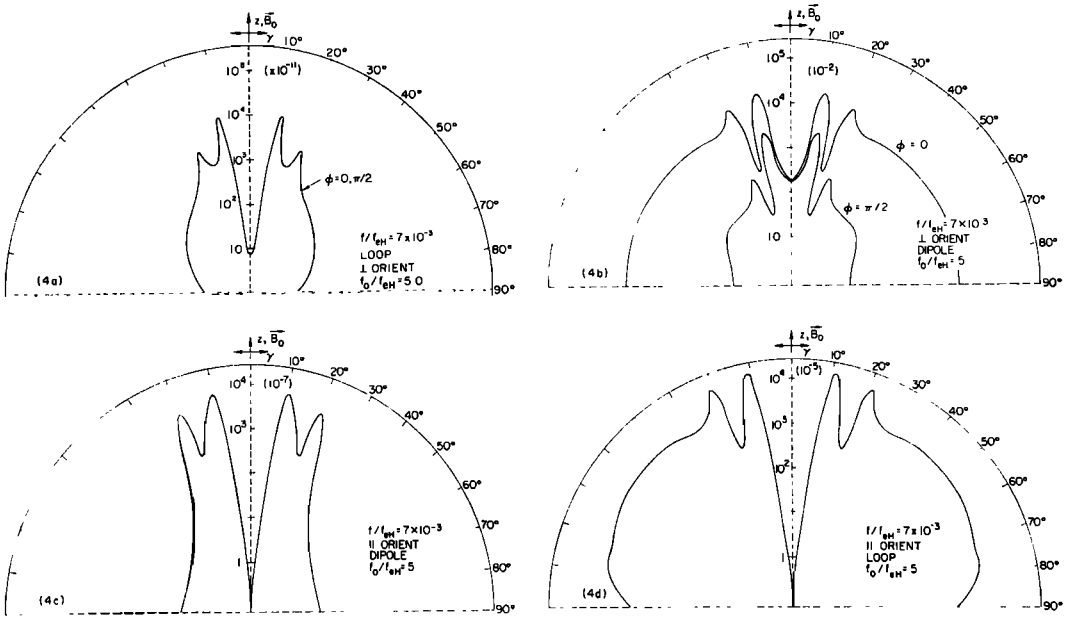

Fig. 4. Normalized radiation patterns for magnetic (L) and electric (D) dipoles for the frequency $f = 7 \times 10^{-3} f_{eH}$. The patterns shown are typical of those that occur in the frequency range $f_{LHR} > f > 4.6 f_{pH}$, assuming a moderate to high density plasma. In this range nonlongitudinal focusing effects produce the major lobes of the pattern.

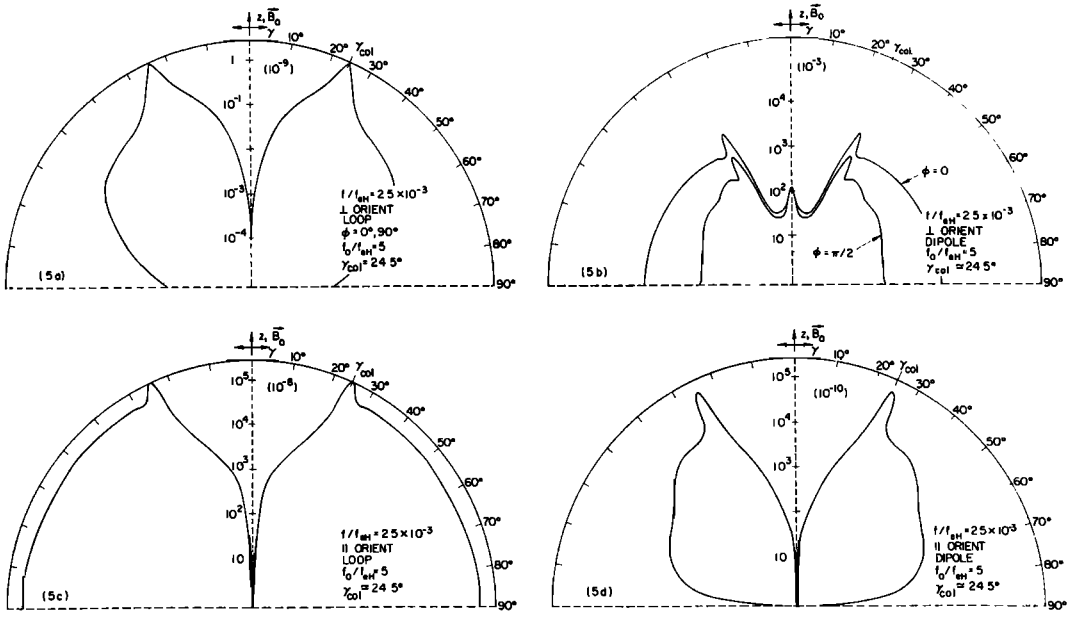

Fig. 5. Normalized radiation patterns for magnetic (L) and electric (D) dipoles for the frequency $f = 2.5 \times 10^{-3} f_{eH}$ ($f = 4.6 f_{pH}$). At this frequency the effects of nonlongitudinal focusing are most pronounced and give rise to the major lobe at $\gamma = 24.5°$. The lobe amplitude increases as $r^{1/2}$ owing to this focusing.

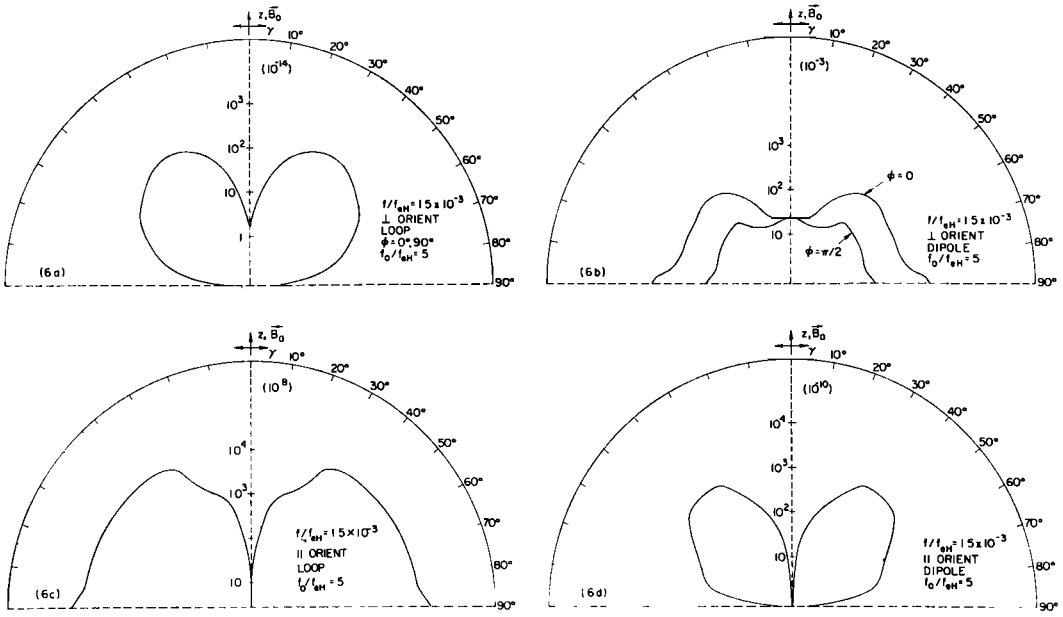

Fig. 6. Normalized radiation patterns for magnetic (L) and electric (D) dipoles for the frequency $f = 1.5 \times 10^{-3} f_{eH}$. The patterns shown are typical of those that occur in the frequency range $4.6 f_{pH} > f \geq f_{pH}$, when a moderate to high density plasma is assumed. In this range, all focusing effects are absent and the radiation varies as r^{-2} for all γ.

found that in all orientations the radiation patterns for magnetic dipoles and electric dipoles are dissimilar in shape and dependence on azimuth.

The normalized dipole radiation patterns for the frequency $f = 1.5 \times 10^{-3} f_{eH}$ are shown in Figure 6. These plots illustrate the type of radiation pattern that occurs in the frequency range $f_{pH} < f < 4.6 f_{pH}$. In this range only one saddle point contributes to the radiation pattern, no inflection points exist on the whistler-mode refractive-index surface, and no focusing effects take place. A typical refractive-index surface in this frequency range is shown in Figure 7*d*. In Figure 6 it is once again seen that the pattern for the magnetic dipoles (Figure 6*a* and *c*) bear little resemblance to the patterns for the electric dipoles (Figure 6*b* and *d*).

Although the plots shown in Figures 1 through 6 apply only to the radiation in the half space $z > 0$, the radiation pattern for $z < 0$ can be easily obtained by reflecting the pattern for $z > 0$ through the source point.

Discussion and Conclusions

A few of the interesting features of the radiation patterns shown in Figures 1 through 6 are summarized below.

1. For frequencies in the range $\frac{1}{2} f_{eH} \geq f > f_{LHR}$, the distribution of radiation is controlled by the longitudinal focusing effect, and the major lobe of the radiation pattern lies along the static magnetic field $\bar{B}_0$. Exceptions to this rule can occur if the dipole symmetry axis lies precisely along $\bar{B}_0$.

2. For frequencies in the range $f_{eH} \geq f \geq f_{LHR}$, where the whistler-mode refractive-index surface is open and the complementary cone of half angle γ_c exists, it is found that a magnetic dipole will radiate a smaller fraction of its energy into angles near γ_c than will an electric dipole. Furthermore, for $\frac{1}{2} f_{eH} \geq f > f_{LHR}$, magnetic dipoles are more efficient in producing radiation along $\bar{B}_0$.

3. For all frequencies in the range $\frac{1}{2} f_{eH} \geq f > 4.6 f_{pH}$, the lobes produced by focusing effects dominate the radiation patterns.

4. For $f_{eH} > f \geq f_{LHR}$, no radiation flows directly across $\bar{B}_0$, the radiation is confined within a cone of half angle γ_L, where γ_L is the larger of the two angles γ_c and γ_m. (See equa-

tion 16 for definition of γ_m.) A plot of γ_L versus f can be found in *Helliwell* [1965].

The features listed above will vary in importance depending on the particular application envisioned for the magnetospheric satellite transmitter. For instance, if one wishes to carry out wave-particle interaction experiments involving particles trapped on field lines that intersect the satellite, then it is important to maximize the radiation along $\bar{B}_0$, and the use of a perpendicular loop antenna at frequencies $\frac{1}{2} f_{eH} \geq f > f_{LHR}$ would seem in order. On the other hand, if a wave-propagation experiment is contemplated in which nonducted modes [*Smith and Angerami*, 1968] are to be studied, it is important to maximize the radiation at high wave-normal angles (i.e., radiation flowing close to the complementary cone) and the use of a parallel electric dipole antenna would seem in order.

Needless to say, in designing a satellite transmitter the radiation pattern alone cannot be used to determine the type of antenna to be used, since attention must also be paid to the antenna radiation efficiency as well as to any undesirable trade-offs between maximum transmitter power output and antenna size and/or configuration. Nevertheless, plots such as those of Figures 1 through 6 are useful in the initial planning of satellite transmitter experiments, and we can broadly interpret our results as indicating at least that focusing effects should be of significant importance in the design of a VLF/ELF satellite transmitting system in the magnetosphere.

The major weakness of the power integral formulation (equation 4) that we have used to find the radiation pattern is the fact that it is useful only when collisional losses are small. This fact is not troublesome when application is made to the magnetosphere at altitudes above a few thousand kilometers, since in this region the effective electron collision frequencies are generally less than 1 per sec, whereas the transmitter operating frequency would generally be many times this. On the other hand, if the transmitter is to operate at much lower altitudes and at ELF frequencies commensurate with the effective electron collision frequency, our formulation will fail and recourse must be made to a more general formulation.

It is interesting to note that in our formulation interference effects in the radiation pattern do not appear when multiple rays make up the power flow in a given direction. In *Kuehl's* [1962] formulation, interference terms appear in the radiation pattern whenever inflection points exist on the whistler-mode refractive-index surface $\bar{n}(\theta)$ and the pattern is made up of multiple rays. These interference effects have been discussed by *Arbel and Felsen* [1963] and *GiaRusso and Bergeson* [1970].

The fact that such interference terms are absent in our formulation shows that these terms do not represent a net radial flow of electromagnetic energy from the antenna.

Although *GiaRusso and Bergeson* [1970] correctly conclude that interference terms will be absent when inflection points no longer exist on $\bar{n}(\theta)$, they imply that the inflection points will vanish whenever $f < f_{LHR}$. Our own results show that the inflection points on $\bar{n}(\theta)$ do not vanish until $f < 4.6\, f_{pH}$, i.e., $f < 10^{-1}\, f_{LHR}$. These authors also appear to imply that at VLF the confinement cone (see item 4 above) disappears when no inflection point exists on $\bar{n}(\theta)$. In reality, a confinement cone exists for all frequencies in the range $f_{eH} \geq f > f_{LHR}$, including those frequencies ($f_{eH} \geq f \geq \frac{1}{2} f_{eH}$) where no inflection points are present on $\bar{n}(\theta)$.

In the present paper we have utilized the power integral method of constructing radiation patterns because we feel that it is a simpler and more convenient method than the usual poynting-vector approach (such as that developed by *Kuehl* [1962]). We have presented this alternate method in the knowledge that the radiation patterns produced by both the poynting-vector method and our own method are identical, with the exception of interference terms. The point-to-point correspondence of the two methods can be demonstrated by the straightforward but tedious mathematical procedure of comparing the radial component of the poynting vector, minus the interference terms (see *GiaRusso and Bergeson* [1970, equation 18]), with our equations 24*a* and 27*a*. Since the interference terms in question can be shown generally to have little effect on the details of the pattern, it is clear that in the situations considered the power integral method and the poynting-vector method have basically the same physical content.

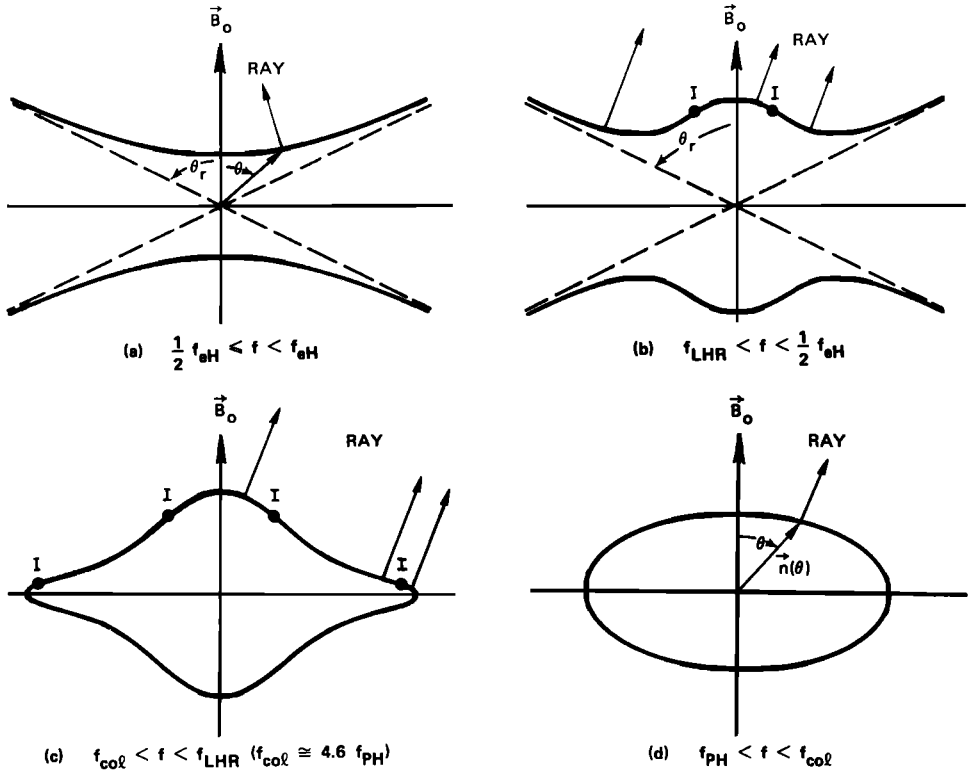

Fig. 7. Typical whistler-mode refractive index surfaces $\bar{n}(\theta)$ for various frequency ranges in the interval $f_{eH} \geq f \geq f_{pH}$. The ray direction appropriate to a particular wave-normal angle θ_0 is given by the normal to $\bar{n}(\theta)$ at θ_0. Presence of inflection points (labeled I) on $\bar{n}(\theta)$ results in illumination of some portions of the observation space by multiple rays. In the lossless case, whenever we have $f_{eH} \geq f \geq f_{LHR}$, we also have $\bar{n}(\theta) \to \infty$ as $\theta \to \theta_r$, where $\theta_r = \tan^{-1} |\epsilon_0/\epsilon_e|$ is the resonance-cone half angle.

On the other hand, we know of no general physical argument that would indicate that the power integral method must always give the correct radiation pattern in an anisotropic plasma. Indeed, as a reviewer has pointed out, any integrand whose integral is 0 could be added to the integrand in (4), and this addition would not alter the value of the integral, although it would certainly alter the radiation pattern.

In view of this consideration, it is perhaps advisable to use the power integral method with caution in new situations.

A final point to note here is the fact that there is presently some controversy over the meaning of the real part of P, as given in (1), in circumstances where the refractive-index surface is open ($f_{LHR} \leq f \leq f_{eH}$) and where the radiating element is an electric dipole. One school of thought contends that in the lossless case the major portion of Re P is due to a quasistatic 'residual resistance' [*Balmain and Oksiutik*, 1969] in the plasma and is not actually due to radiation. It is usually argued that the residual-resistance phenomenon occurs because the intense power that one finds near the complementary cone for an electric dipole consists of nonpropagating near-field energy rather than propagating far-field energy. The merits of this argument appear questionable for the main reason that it is based entirely on quasistatic theory that itself is clearly not applicable when the refractive-index surface is open. Nevertheless, we wish to point out that the usefulness of our electric dipole radiation plots can in no way depend on the existence or nonexistence of a 'residual-resistance' effect, since, for reasons

stated in the preceding section, we have already specifically denied physical meaning to the power flow near the complementary cone.

Acknowledgments. The authors gratefully acknowledge the support and encouragement of Professor R. A. Helliwell and the Radioscience Laboratory staff during the course of this research.

The work of one of us (T.F.B.) was supported by the National Aeronautics and Space Administration under grant NgL-008. The work of the other (T.N.C.W.) was supported in part by the National Aeronautics and Space Administration under grant NgL-008 and in part by Stanford Research Institute Internal Research Funds.

* * *

The Editor thanks H. Weil and another referee for their assistance in evaluating this paper.

References

Arbel, E., and L. B. Felsen, Theory of radiation from sources in an anisotropic media, in *Proceedings of the Symposium on Electromagnetic Theory and Antennas*, part 2, edited by E. C. Jordan, pp. 421–459, Pergamon, New York, 1963.

Balmain, K. G., and G. A. Oksiutik, R.F. probe admittance in the ionosphere, in *Plasma Waves in Space and Laboratory*, pp. 241–261, Edinburgh University Press, Edinburgh, 1969.

Bunkin, F. V., On radiation in anisotropic media. Sov. Phys. *JETP*, Engl. Transl., *32*, 338–346, 1957.

Felsen, L. B., On the use of refractive index diagrams for source-excited anisotropic regions, *Radio Sci., 69D*, 155–169, 1965.

Freire, G. F., and R. R. Scarabucci, Radiation from an electric dipole immersed in a lossy anisotropic plasma, *Int. J. Electron., 22*, 65–80, 1967.

GiaRusso, D. P., and J. E. Bergeson, Studies of VLF radiation patterns of a dipole immersed in a slightly lossy magnetoplasma, *Radio Sci., 5*, 745–766, 1970.

Helliwell, R. A., *Whistlers and Related Ionospheric Phenomena*, p. 36, Stanford University Press, Palo Alto, Calif., 1965.

Kogelnik, H., and H. Motz, Electromagnetic radiation from sources embedded in an infinite anisotropic medium and the significance of the poynting vector, in *Proceedings of the Symposium on Electromagnetic Theory and Antennas*, part 1, edited by E. C. Jordan, pp. 477–493, Pergamon, New York, 1963.

Kuehl, H. H., Electromagnetic radiation from an electric dipole in a cold anisotropic plasma, *Phys. Fluids, 5*, 1095–1103, 1962.

Lighthill, M. J., Studies on magneto-hydrodynamic waves and other anisotropic wave motion, *Phil. Trans. Roy. Soc., London, A, 252*, 397–430, 1960.

Mittra, R., and G. A. Deschamps, Field solution for a dipole in an anisotropic medium, in *Proceedings of the Symposium on Electromagnetic Theory and Antennas*, edited by E. C. Jordan, pp. 495–512, Pergamon, New York, 1963.

Mittra, R., and G. L. Duff, A systematic study of the radiation patterns of a dipole in a magnetoplasma based on a classification of the associated dispersion surfaces, *Radio Sci., 69D*, 681–692, 1965.

Smith, R. L., and J. J. Angerami, Magnetospheric properties deduced from Ogo 1 observations of ducted and nonducted whistlers, *J. Geophys. Res., 73*, 1–20, 1968.

Snyder, M. A., and H. Weitzner, VLF electromagnetic radiation in a magnetoionic medium, *Radio Sci., 3*, 943–954, 1968.

Staras, H., The impedance of an electric dipole in a magnetoionic medium, *IEEE Trans. Antennas Propagat., AP-12*, 695–702, 1964.

Wang, T. N. C., and T. F. Bell, On VLF radiation fields along the static magnetic field from sources immersed in a magnetoplasma, *Trans. IEEE Antennas Propagat., AP-17*, 824–827, November 1969*a*.

Wang, T. N. C., and T. F. Bell, Radiation resistance of a short dipole immersed in a cold magnetoionic medium, *Radio Sci., 4*, 167, 1969*b*.

Wang, T. N. C., and T. F. Bell, VLF/ELF input impedance of an arbitrarily oriented strip-loop antenna in a multicomponent magnetoplasma, *IEEE Trans. Antennas Propagat.*, in press, 1972.

Wu, C. P., Radiation from dipoles in a magnetoionic medium, *IEEE Trans. Antennas Propagat., AP-11*, 681, 1963.

(Received August 13, 1971;
accepted December 2, 1971.)